The EMBO Journal (2005) 24, 2342–2353 | © 2005 European Molecular Biology Organization | All Rights Reserved 0261-4189/05
www.embojournal.org

THE EMBO JOURNAL

VEGF receptor-2 Y951 signaling and a role for the adapter molecule TSAd in tumor angiogenesis

Taro Matsumoto[1,2], Svante Bohman[1], Johan Dixelius[1], Tone Berge[3], Anna Dimberg[1], Peetra Magnusson[1], Ling Wang[4], Charlotte Wikner[1], Jian Hua Qi[5], Christer Wernstedt[6], Jiong Wu[7], Skjalg Bruheim[8], Hideo Mugishima[2], Debrabata Mukhopadhyay[4], Anne Spurkland[3] and Lena Claesson-Welsh[1,*]

[1]Rudbeck Laboratory, Department of Genetics and Pathology, Uppsala University, Uppsala, Sweden, [2]Division of Cell Regeneration and Transplantation, Advanced Medical Research Center, Nihon University School of Medicine, Ohyaguchikamimachi, Itabashi-ku, Tokyo, Japan, [3]Department of Anatomy, Institute of Basal Medical Sciences, University of Oslo, Blindern, Oslo, Norway, [4]Mayo Clinic Foundation, Gugg, Rochester, MN, USA, [5]Department of Ophthalmic Research, Cole Eye Institute, Cleveland Clinic Foundation, Cleveland, OH, USA, [6]Ludwig Institute for Cancer Research, Uppsala Branch, Biomedical Center, Uppsala, Sweden, [7]Cell Signaling Technology, Cummings Center, Beverly, MA, USA and [8]Department of Tumor Biology, Institute for Cancer Research, The Norwegian Radium Hospital, Oslo, Norway

Vascular endothelial growth factor receptor-2 (VEGFR-2) activation by VEGF-A is essential in vasculogenesis and angiogenesis. We have generated a pan-phosphorylation site map of VEGFR-2 and identified one major tyrosine phosphorylation site in the kinase insert (Y951), in addition to two major sites in the C-terminal tail (Y1175 and Y1214). In developing vessels, phosphorylation of Y1175 and Y1214 was detected in all VEGFR-2-expressing endothelial cells, whereas phosphorylation of Y951 was identified in a subset of vessels. Phosphorylated Y951 bound the T-cell-specific adapter (TSAd), which was expressed in tumor vessels. Mutation of Y951 to F and introduction of phosphorylated Y951 peptide or TSAd siRNA into endothelial cells blocked VEGF-A-induced actin stress fibers and migration, but not mitogenesis. Tumor vascularization and growth was reduced in TSAd-deficient mice, indicating a critical role of Y951-TSAd signaling in pathological angiogenesis.

The EMBO Journal (2005) **24,** 2342–2353. doi:10.1038/sj.emboj.7600709; Published online 16 June 2005
Subject Categories: signal transduction; molecular biology of disease
Keywords: actin cytoskeleton; TSAd; tumor angiogenesis; tyrosine phosphorylation site; VEGFR-2

*Corresponding author. Rudbeck Laboratory, Department of Genetics and Pathology, Uppsala University, Dag Hammarskjöldsv. 20, 75185 Uppsala, Sweden. Tel.: +46 18 471 43 63; Fax: +46 18 55 89 31; E-mail: lena.claesson-welsh@genpat.uu.se

Received: 3 November 2004; accepted: 18 May 2005; published online: 16 June 2005

Introduction

Vascular endothelial growth factor (VEGF)-A/vascular permeability factor (VPF) is critical for vascular development and angiogenesis, that is, formation of new blood vessels from existing capillaries (Ferrara, 2002). VEGF-A is distinguished by its potent regulation by hypoxia and its occurrence in several splice variants that to different extents bind to heparan sulfate and to the extracellular matrix. Moreover, deletion of only one allele of the *VEGF-A* gene leads to embryonic lethality resulting from arrest in vascular development (for a review, see Matsumoto and Claesson-Welsh, 2001). The critical involvement of VEGF-A in vascular development and angiogenesis occurs through binding and activation of VEGF receptor-2 (VEGFR-2). VEGFR-2 is essential for endothelial cell function and is the earliest known marker for vascular endothelial cells (Kabrun *et al*, 1997). Inactivation of the *VEGFR-2* gene leads to a phenotype similar to that produced by VEGF-A deletion, with early embryonic death resulting from lack of proper differentiation and/or proper localization of endothelial cells (Matsumoto and Claesson-Welsh, 2001).

A growing number of diseases, such as cancer, chronic inflammation, and diabetic retinopathy, are characterized by excess angiogenesis. Progression of these diseases may depend on the attraction of blood vessels to oxygenate and nurture the growing tissue. Tumor cells often produce VEGF-A, and, in models of multistage tumor disease, onset of angiogenesis is a prerequisite for the switch from a dysplastic lesion to an expanding malignancy (the angiogenic switch; for a review, see Hanahan and Folkman, 1996).

The VEGFR-2 kinase is activated according to the consensus scheme for tyrosine kinases; binding of the dimeric VEGF-A to the extracellular domains of two monomeric receptors induces dimerization and activation of the tyrosine kinase. Certain aspects of the signal-transduction properties of the VEGFR-2 kinase have been analyzed in depth. Tyrosine residues Y1054 and Y1059 in the kinase domain serve as positive regulatory sites (Dougher and Terman, 1999; Kendall *et al*, 1999). Phosphorylation at Y1175 in the VEGFR-2 C-terminal tail allows binding, phosphorylation, and activation of phospholipase Cγ1 (PLCγ_1) (Takahashi *et al*, 2001), ultimately leading to Ca^{2+} influx and activation of protein kinase C. Phosphorylated Y1175 also binds the adapter molecule Shb, which mediates activation of phosphoinositide 3′ kinase (PI3-kinase) and assembly of focal adhesions (Holmqvist *et al*, 2004). Exchange of Y1175 for F in the *VEGFR-2* gene results in a loss-of-function phenotype and embryonic lethality (Sakurai *et al*, 2005). Phosphorylation at other sites, such as Y951 in the kinase insert, has been inferred from analyses of bacterially expressed VEGFR-2 intracellular domain (Dougher-Vermazen *et al*, 1994); by mutational analyses, Y951 has been linked to migration of endothelial cells (Zeng *et al*, 2001). Using a two-hybrid screen in yeast, Wu *et al* (2000) identified an adapter molecule

designated VEGF receptor-associated protein (VRAP) as a binding partner to Y951. VRAP is equivalent to the T cell-specific adapter molecule (TSAd)/Rlk and Itk-binding protein (RIBP)/Lck adapter (LAD), which we have designated TSAd in this study. *TSAd* gene inactivation results in impaired T-cell-receptor activation and immune-response deficiency (Rajagopal *et al*, 1999).

The overall objective of this study was to create a pan-phosphorylation map of VEGFR-2 and to determine the roles of the phosphorylation sites in endothelial cell function *in vivo*. For this purpose, we have determined phosphorylation sites in VEGFR-2 under conditions that allow resolution of all possible sites except Y1175, which is a previously identified phosphorylation site in VEGFR-2. Thereby, a pan-phosphorylation site map of VEGFR-2 can be constructed, with five major phosphorylation sites: Y951 in the kinase insert; Y1054 and Y1059 in the C-terminal part of the kinase domain; Y1175 and Y1214 in the C-terminal tail. We show that Y951 is used only in certain endothelial cells during development and that phosphorylated Y951 binds and mediates tyrosine phosphorylation of TSAd, which is expressed in endothelial cells in tumor vasculature. Moreover, we show that Y951-mediated coupling of VEGFR-2 and TSAd is critical for VEGF-A-mediated actin reorganization in endothelial cells and for tumor vascularization and growth.

Results

Phosphorylation of tyrosine residues in VEGFR-2

The intracellular domain of VEGFR-2 contains 19 tyrosine residues, 11 of which are located in the noncatalytic part of the receptor, potentially serving as phosphorylation sites (Figure 1A). To create a pan-phosphorylation site map of VEGFR-2, we labeled immunoprecipitated VEGFR-2 using γ-^{32}P-ATP in a kinase reaction; we have shown that this procedure faithfully mimics phosphorylation in intact cells (Ito *et al*, 1998; Dixelius *et al*, 2003). The ^{32}P-labeled VEGFR-2 sample was digested with trypsin, and the digest was separated in two dimensions by electrophoresis and liquid chromatography. This approach allows resolution of all potential phosphotyrosine-containing VEGFR-2 tryptic peptides except the one encompassing Y1175 (Figure 1A) that is negatively charged under the employed conditions. The resulting phosphopeptide map is shown in Figure 1B. A number of phosphopeptides (indicated as spots a–h in the schematic representation in Figure 1B) were reproducibly identified. Phosphoamino-acid analyses showed that spots a–f contained phosphotyrosine, whereas spots g and h contained phosphoserine and phosphothreonine (Figure 1C).

To determine the positions of ^{32}P-tyrosine residues, peptides eluted from phosphotyrosine-containing spots were subjected to radiochemical sequencing. As seen in Figure 1D, sequencing of peptides from spots a, b, and c resulted in elution of radioactive residues in position 2 (spot a) and position 3 (spots b and c). This outcome allowed the tentative assignment of spot a as the phosphoY951 (pY951)-containing peptide. Similarly, spots b and c most likely corresponded to pY1054- and/or pY1214-containing peptides. To confirm spot a as pY951 and to distinguish between pY1054 and pY1214, Y-to-F mutations in VEGFR-2 were created and phosphopeptide maps were produced as described above. We thereby confirmed that spot a corresponded to pY951 and showed that spots b and c corresponded to pY1054 and pY1214, respectively (Figure 1D). The tryptic peptide encompassing pY1214 also contains Y1223, which if phosphorylated should give rise to a peak in cycle 12. This peak was missing; moreover, the Y1214F mutant completely lacked spot c. Phosphorylation at Y1223 should have been noticed as a persistent, albeit less intense, spot c slightly shifted upwards and to the left. As a control, we generated a phosphopeptide map of a VEGFR-2 Y996F mutant, in which all phosphopeptide spots seen in the wild-type (Wt) map were retained (bottom panel in Figure 1D).

The identity of spots d–f was sought with similar strategies. However, no radioactive peaks were obtained when subjecting spots d and e to 20 consecutive Edman degradation cycles. Re-cleavage of the d and e tryptic peptides with cyanogen bromide or endoproteinase Asp-N also did not result in interpretable sequences (data not shown). Nevertheless, we noted that a truncated VEGFR-2 lacking five tyrosine residues of the six in the C-terminal tail (Ct truncated) did not give rise to spots d and e in the phosphopeptide map (Figure 1E). In addition, spot c was missing, which is compatible with the assignment of this spot as pY1214. We therefore examined the contribution of Y1305, Y1309, and Y1319 to spots d and e. A triple mutant carrying F instead of Y at all three positions also lacked spots d and e (Figure 1E). In contrast, individual mutations at these sites still allowed phosphorylation at d and e, but showed changes in the mobility of weakly labeled ^{32}P-peptides, which were not amenable to radioactive Edman degradation (data not shown). Our interpretation of these data is that the C-terminal Y1305, Y1309, and Y1319 are phosphorylated only at a low stoichiometry after VEGF-A stimulation. By mutation of all three sites, the folding of the C-terminal tail may be disturbed, which in turn affects the accessibility to the VEGFR-2 kinase of other sites most likely in the kinase domain.

Sequencing of spot f showed multiple radioactive peaks in repeated experiments, most likely because of incomplete cleavage at certain potential cleavage sites. However, the migration position of spot f fits with that of Y1059, which, previously, has been identified as a phosphorylation site (Dougher and Terman, 1999; Kendall *et al*, 1999). Mutation of Y1059 to F renders the receptor kinase inactive (Zeng *et al*, 2001), and we were therefore unable to definitively demonstrate phosphorylation of Y1059 and its assignment as spot f.

Thus, in conclusion, individual mutations of Y951, Y1054 and Y1214 showed that these are major phosphorylation sites in VEGFR-2. The three C-terminal sites Y1305, Y1309, and Y1319 are phosphorylated only to a minor extent, yielding phosphopeptide spots visible after prolonged exposure. Furthermore, we did not see any changes in the VEGFR-2 phosphopeptide map when we analyzed individual Y-to-F mutations at Y801 and Y822 in the juxtamembrane domain and Y938 and Y996 in the kinase insert (see Figure 1F for a summary of the mapping data).

Phosphorylation of VEGFR-2 at Y951, Y1175, and Y1214 in embryoid body (EB) vessels

To demonstrate phosphorylation of VEGFR-2 in intact endothelial cells, we employed phospho-specific antibodies raised against the individual sites to stain vessel structures

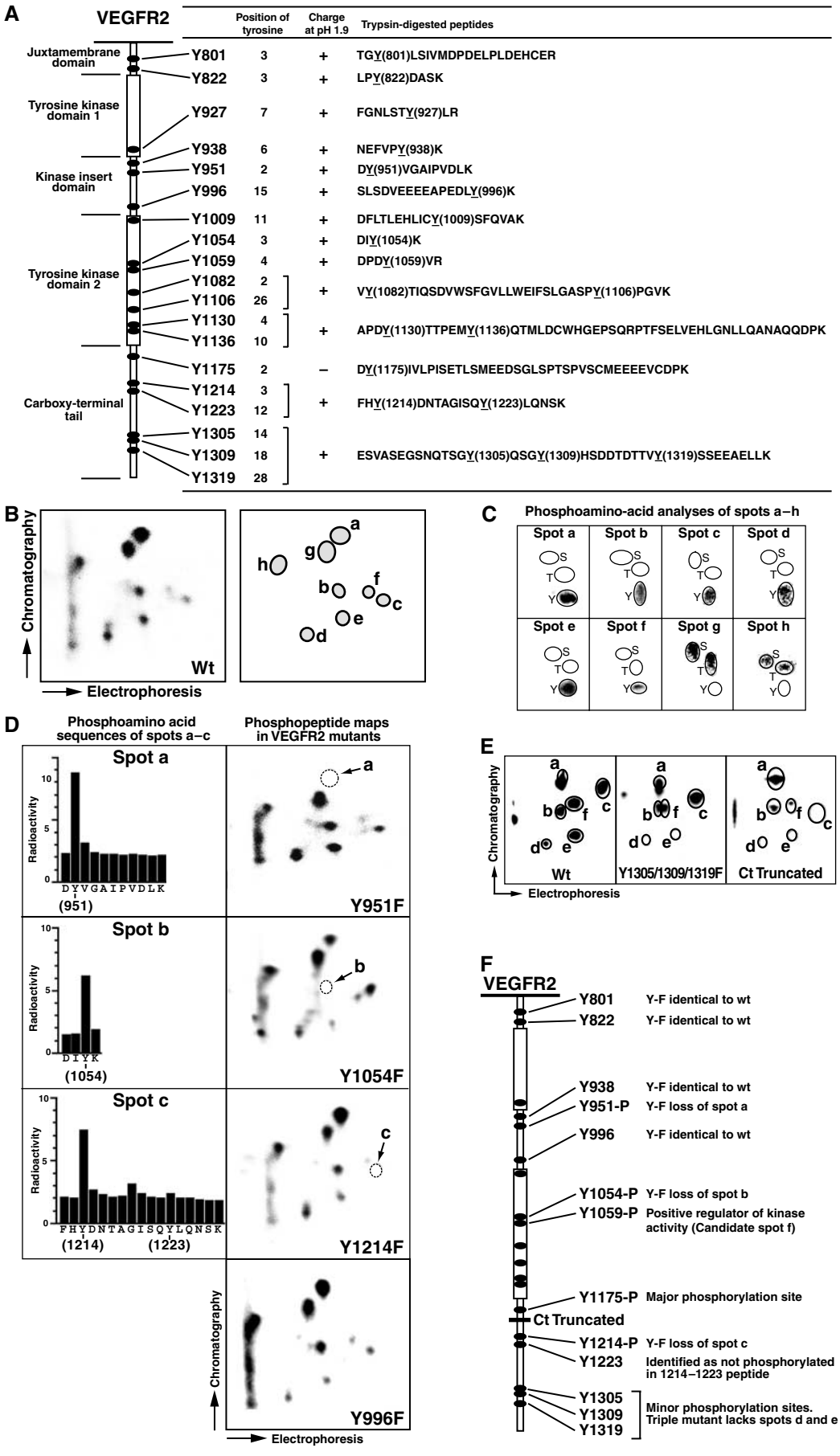

in EBs (see online Supplementary Figure 1 for characterization of the specificity of the phosphosite-specific antibodies). Murine embryonic stem cells (R1) were aggregated in hanging drops to create EBs. We and others have previously documented vascular development in EBs, with spatial and temporal expression patterns of endothelial cell markers very closely mimicking *in vivo* patterns (Magnusson *et al*, 2004). Thus, 8 days after leukemia inhibitory factor (LIF) withdrawal, which allowed differentiation of endothelial cells, vessel-like structures expressing CD31 and VEGFR-2 were formed in response to treatment with VEGF-A (Figure 2A). Costaining with antibodies against the VEGFR-2 protein and the phosphosite-specific antibodies against pY1175 or pY1214 showed that, wherever VEGFR-2 was expressed, it was phosphorylated at these two positions (Figure 2B). In contrast, some but not all of the VEGFR-2-expressing vessels were positive for phosphorylation at Y951 (Figure 2B, bottom panel). Costaining of EBs with antibodies against VEGFR-2 protein, pY951, and α-smooth muscle cell actin (ASMA) showed that endothelial cells lacking VEGFR-2 phosphorylated at Y951 more often were covered by pericyte-like, ASMA-positive cells, whereas endothelial cells containing VEGFR-2 phosphorylated at Y951 lacked associated pericytes (Figure 2C).

pY951 regulates actin reorganization downstream of VEGFR-2

To determine which VEGF-A-induced signals are transduced via pY951 in VEGFR-2, we generated stable porcine aortic endothelial (PAE) cell lines expressing Wt VEGFR-2, mutated Y951F VEGFR-2, or, as a control, Y996F VEGFR-2. These lines were examined by immunoblotting and phosphatidyl inositol phosphate assay for the capacity to mediate the VEGF-A signal to known VEGFR-2 downstream targets such as extracellular regulated kinase (ERK), p38 mitogen-activated protein kinase (p38 MAPK), PLCγ_1, and PI3-kinase/Akt pathways. However, no difference was detected in activation of these pathways between cells expressing the Wt VEGFR-2 or the mutants Y951F and Y996F (data not shown).

VEGF-A is known to stimulate DNA synthesis and cell migration, involving actin stress fiber reorganization. We sought a role for Y951 in VEGF-A signal transduction regulating these responses by introduction of biotinylated, phosphorylated Y951 peptide, or the unphosphorylated counterpart as a control into human umbilical vein endothelial (HUVE) cells. The cells were stimulated with VEGF-A and stained with TRITC-phalloidin to visualize the actin cytoskeleton. VEGF-A treatment induced formation of stress fibers in untreated cells and in cells transfected with the unphosphorylated peptide (Figure 3A). In contrast, VEGF-A-induced actin stress fiber formation was blocked to basal level in cells containing the phosphorylated Y951 peptide (Figure 3A and B). Staining of cells by FITC-coupled streptavidin showed that most cells in the culture were successfully transfected; moreover, staining with phosphotyrosine antibodies revealed that phosphorylation remained for about 120 min after transfection (see Supplementary Figure 2). We therefore argued that VEGF signals dependent on pY951 would be efficiently blocked for up to 2 h, allowing analysis of long-term responses to VEGF, such as DNA synthesis. Thus, whereas VEGF-A-induced actin reorganization was blocked by the pY951 peptide to a level seen in unstimulated cells (Figure 3B), incorporation of BrdU was not significantly affected by introduction of the peptide (Figure 3C). To show that the Y951-dependent effect on actin stress fiber formation represents a motility response, we employed primary HUVE cells transduced with retrovirus encoding a fusion protein composed of the epidermal growth factor receptor (EGFR) extracellular domain fused to the transmembrane and intracellular part of VEGFR-2 of either Wt or mutant Y951F forms, designated EGDR and Y951F EGDR, respectively (see online Supplementary Figure 3 for characterization of EGDR and Y951F EGDR HUVE cells). We have previously shown that the Y951F EGDR-expressing HUVE cells undergo proliferation in response to EGF to the same extent as Wt EGDR cells (Zeng *et al*, 2001). A wound assay was performed which showed that EGF-treated HUVE cells expressing Wt EGDR migrated to fill the wounded cell monolayer over a 24-h time period (Figure 3D), whereas the mutant Y951F EGDR-expressing cells failed to respond to EGF in this assay (Figure 3E).

TSAd signals downstream of pY951

An adapter molecule denoted TSAd/RIBP/Lad/VRAP has been implicated as a binding partner of VEGFR-2/Y951 in a yeast two-hybrid screen (Wu *et al*, 2000). TSAd was initially discovered in T lymphocytes and is highly expressed in peripheral blood mononuclear cells (PBMC) (Spurkland *et al*, 1998). The use of TSAd-specific nucleotide oligomers allowed PCR amplification of fragments from PBMC as well as from HUVE cells (see Supplementary Figure 4). Analysis of expression levels of TSAd protein in resting and activated PBMC in comparison to control and VEGF-A-treated HUVE

Figure 1 Generation of a pan-phosphorylation site map of VEGFR-2. (**A**) Schematic drawing of the VEGFR-2 intracellular domain. The 19 tyrosine residues in the intracellular domain are indicated by their amino-acid sequence numbers. Tryptic digestion of VEGFR-2 potentially generates 14 tryptic peptides from the intracellular domain. The electrophoretic migration of these peptides depends on their charge at pH 1.9. (**B**) Tryptic phosphopeptide map of ^{32}P-labeled VEGF-A-stimulated VEGFR-2 at pH 1.9. Tryptic peptides of immunoprecipitated and ^{32}P-labeled VEGFR-2 were separated by electrophoresis in the first dimension and by liquid chromatography in the second dimension. Tryptic phosphopeptide map of Wt VEGFR-2 (left) and schematic representation of the map with spots indicated by letters a–h (right). (**C**) Phosphoamino-acid analyses of all major phosphorylated spots showing phosphorylation on tyrosine in spots a–f and on serine and threonine in spots g and h. (**D**) Phosphopeptide maps of VEGFR-2 mutated at indicated tyrosine residues (Y951F, Y1054F, and Y1214F) to the right shows loss of spots a, b, and c, respectively (indicated by arrows). Phosphopeptide map of mutant Y996F is identical to that of Wt VEGFR-2. The identities of spots a, b, and c were confirmed by radiochemical sequencing of the peptides, shown to the left for each spot, which yielded peaks of radioactivity in the fraction corresponding to the position of the tyrosine residue in each peptide. (**E**) Phosphopeptide maps of Wt VEGFR-2, a triple-mutated Y1305/1309/1319F VEGFR-2, and a C-terminally truncated VEGFR-2 (Ct truncated). Note the absence of spots d and e in the triple mutant map and the additional loss of spot c (Y1214) in the truncated mutant map. (**F**) Schematic drawing of VEGFR-2 with potential phosphorylation sites of the receptor. P indicates major phosphorylation sites. 'Y-F identical to wt' indicates that a mutated VEGFR-2 with a Y-to-F replacement at the particular residue showed the same phosphopeptide map pattern as Wt VEGFR-2 and therefore does not constitute a phosphorylation site.

cells showed that the TSAd protein was expressed at levels in HUVE cells similar to those in activated PBMC and that TSAd expression in HUVE cells was unaffected by VEGF-A treatment (see Supplementary Figure 4).

Using PAE cells expressing Wt VEGFR-2 or mutated Y951F VEGFR-2, we noted that TSAd and Wt VEGFR-2 engaged in a transient complex in response to VEGF-A (Figure 4A), which was lost in the Y951F VEGFR-2-expressing cells, thus validat-

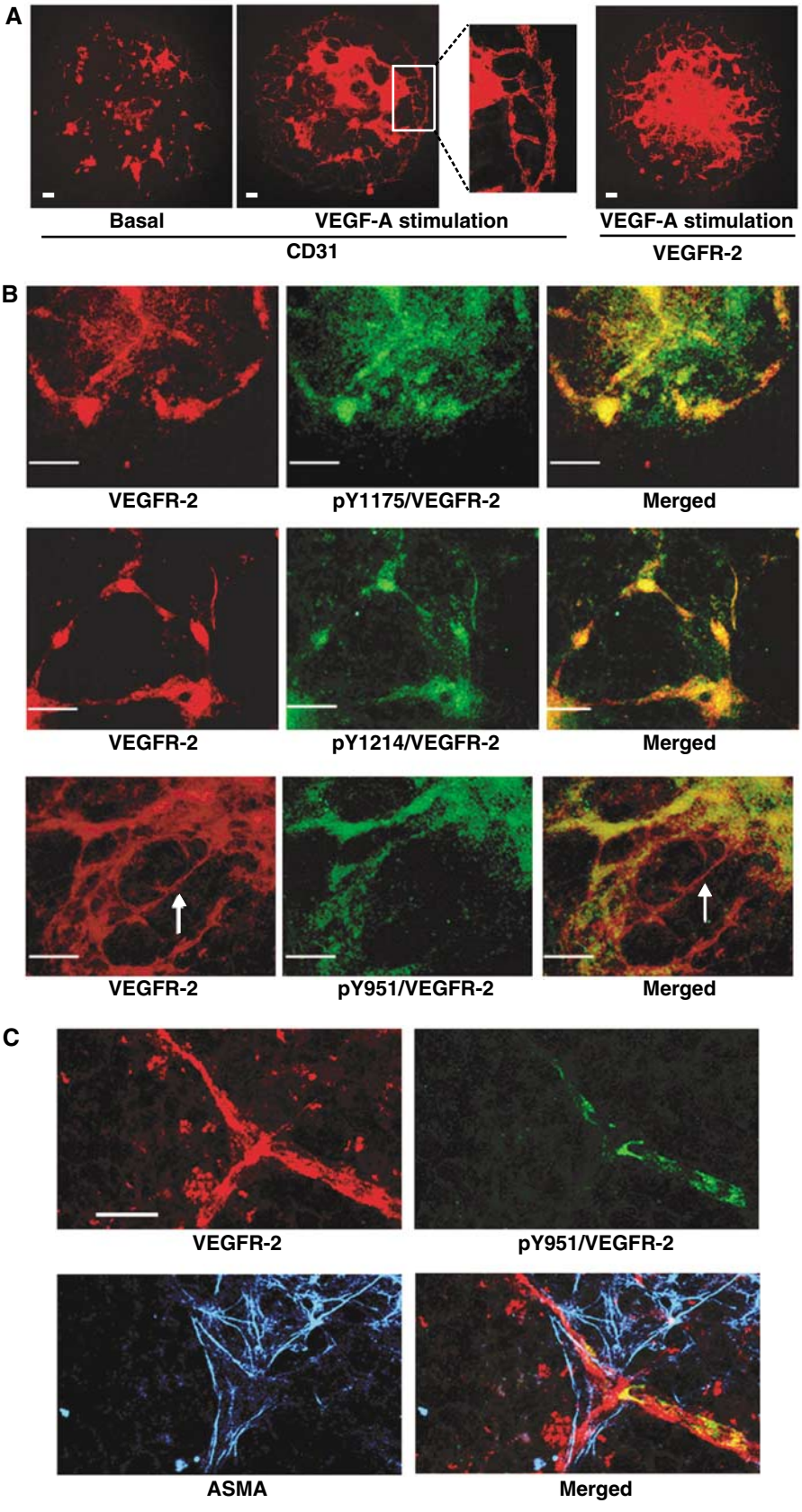

ing previous data (Wu *et al*, 2000). We also used HUVE cells expressing EGDR and Y951F EGDR to show pY951-dependent complex formation between TSAd and VEGFR-2 (see Supplementary Figure 3). VEGF-A treatment induced tyrosine phosphorylation of TSAd in primary HUVE cells (Figure 4B). Transient VEGF-A-induced complex formation between VEGFR-2 and TSAd was detected both after immunoprecipitation (IP) of TSAd followed by blotting for VEGFR-2, and after IP of VEGFR-2 followed by blotting for TSAd. VEGF-A stimulation also mediated an enhanced complex formation between Src and TSAd.

We next examined whether the loss of VEGF-A-induced actin stress fiber formation and motility in the absence of Y951 phosphorylation (Figure 3) resulted from loss of coupling of TSAd to Y951 in VEGFR-2. Expression of TSAd in HUVE cells was suppressed by introduction of TSAd-specific siRNA. RT–PCR of TSAd transcript levels showed a complete loss of transcripts after introduction of 50 nM TSAd siRNA

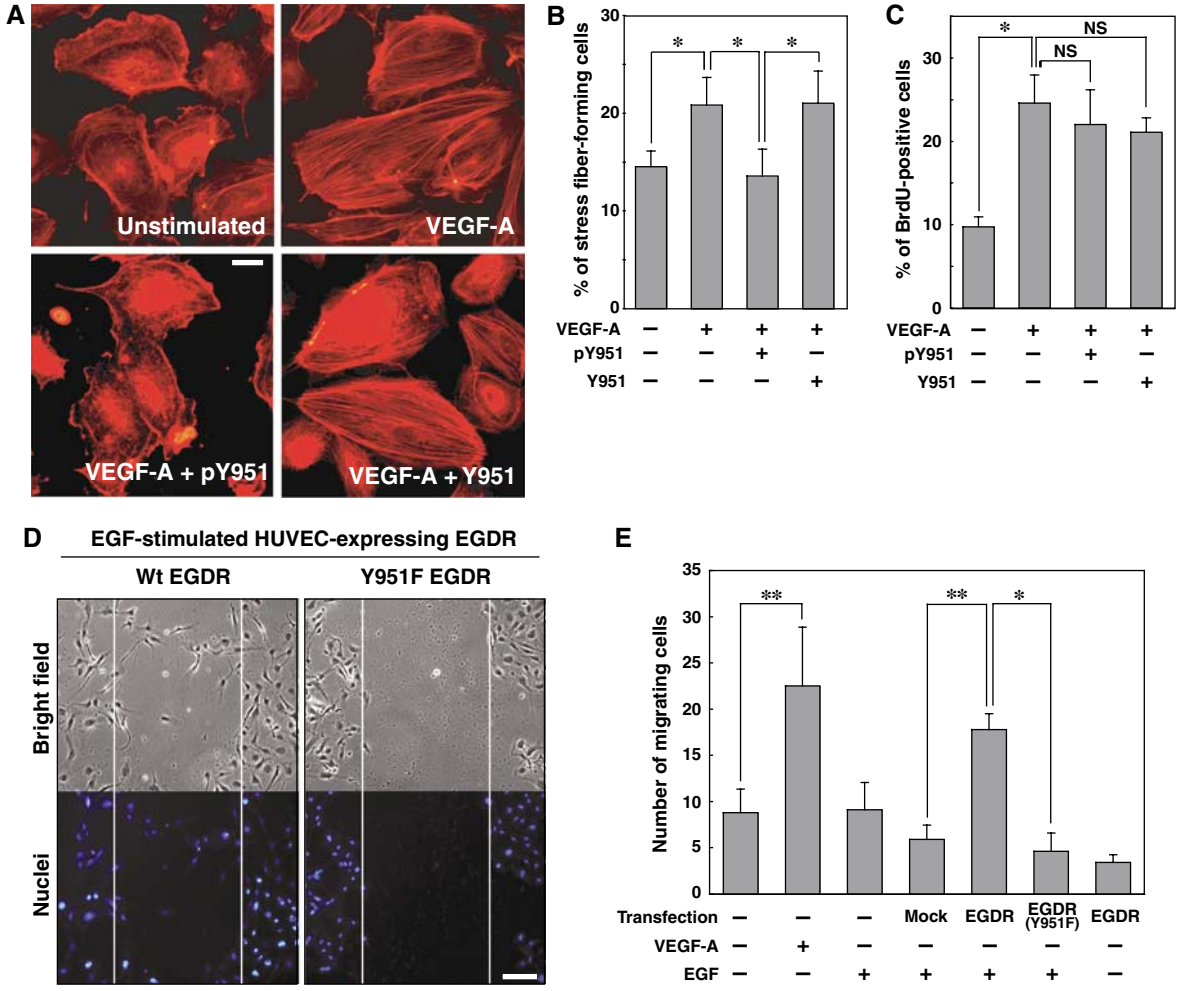

Figure 3 Role of VEGFR-2 Y951 in VEGF-A-induced motility and mitogenicity responses. (**A**) HUVE cells were transfected or not with phosphorylated or unphosphorylated peptide covering Y951 in VEGFR-2. Visualization of actin filaments by TRITC-phalloidin showed stress fiber formation in response to VEGF-A (15 min at 37°C) and block of the response in cells containing the pY951 peptide. Bar: 10 μm. (**B**) Quantification of the fraction of stress fiber-forming cells. Similar results were obtained in two independent experiments. Note that there was a significant decline of VEGF-A-mediated stress fiber formation in pY951 peptide-treated cells. (**C**) VEGF-A-induced BrdU incorporation was similar in HUVE cells transfected with pY951 or Y951 peptides. (**D**) EGF-induced wound closure in HUVE cell monolayer after transduction with retrovirus encoding the EGF receptor/VEGFR-2 fusion protein (EGDR), Wt or Y951F forms. Bar: 250 μm. (**E**) Quantification of the number of cells moving into the wounded area in (D). Similar results were obtained twice in independent experiments. In panels B, C and E, * indicates $P<0.05$, and ** indicates $P<0.01$ (Mann–Whitney *U*-test). NS = not significant. Bars show mean ± s.d. of triplicate wells.

Figure 2 Selective tyrosine phosphorylation at Y951 in VEGFR-2 during vascular development. (**A**) Visualization of the vascular tree in EBs cultured for 8 days in the absence (Basal) and presence of VEGF-A and immunostained to detect vessels using antibodies against CD31 or VEGFR-2. (**B**) VEGF-A-treated EBs coimmunostained with antibodies against VEGFR-2 (red) and pY1175 (green; upper panel) or VEGFR-2 (red) and pY1214 (green; middle panel). To the right in each panel a merged picture is shown, indicating that VEGFR-2 is phosphorylated at Y1175 and Y1214 in all cells expressing the receptor. EBs immunostained with antibodies against VEGFR-2 (red) and pY951 (green; lower panel) show detection of pY951 only in a subset of vessels (arrow; see merged picture to the right). (**C**) Costaining of EBs with VEGFR-2 (red), pY951 (green), and ASMA (blue) show that VEGFR-2-positive vessel structures surrounded by ASMA-positive pericytes lack phosphorylation at Y951. Bars: 100 μm.

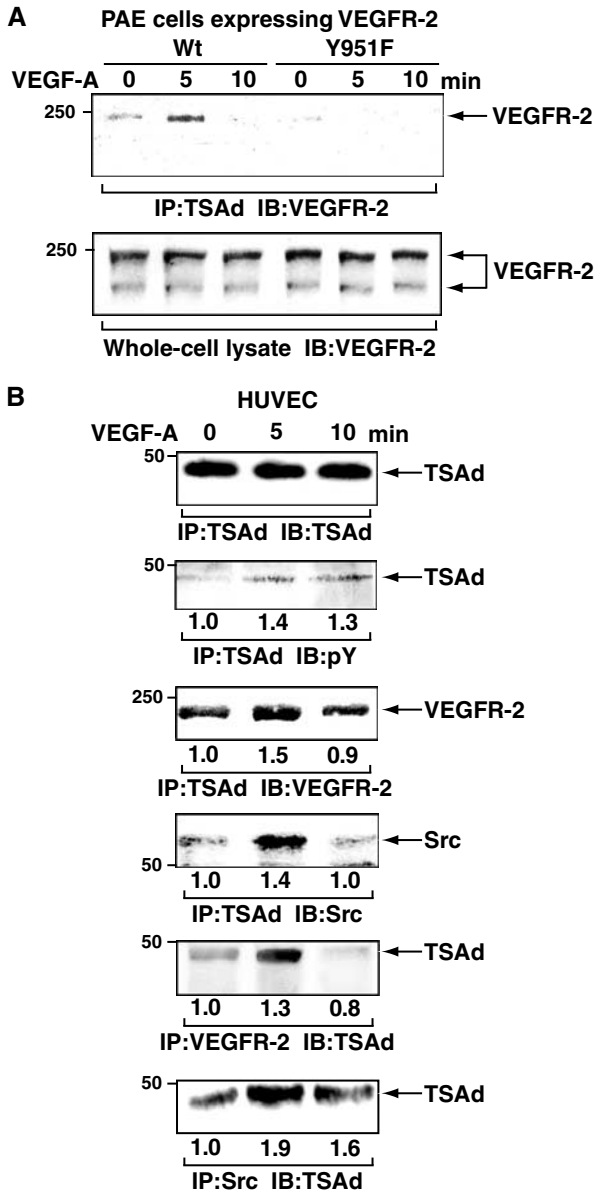

Figure 4 Complex formation and tyrosine phosphorylation of TSAd. (**A**) TSAd/VEGFR-2 complex formation in PAE cells expressing Wt VEGFR-2 or the Y951F mutant receptor (Y951F). Cells were stimulated with VEGF-A or not for 5 or 10 min and processed for immunoprecipitation (IP) of TSAd and immunoblotting (IB) for VEGFR-2. Whole-cell lysate aliquots were blotted for VEGFR-2 to show equal loading of protein. (**B**) HUVE cells treated with VEGF-A or not for 5 or 10 min were analyzed for complex formation between TSAd and VEGFR-2 or Src by IP and IB, as indicated. The relative migration rate of protein standards is shown to the left. The relative changes in band intensity are given below each blot. Note the VEGF-A-induced tyrosine phosphorylation of TSAd and complex formation between VEGFR-2 and TSAd, as well as TSAd and Src.

(see Supplementary Figure 5). HUVE cells that received TSAd siRNA failed to form stress fibers in response to VEGF-A, whereas cells receiving the control, scrambled siRNA showed a potent response (Figure 5A; see Figure 5B for quantification). Furthermore, introduction of the TSAd-specific siRNA suppressed the ability of HUVE cells to respond to VEGF-A in the wound assay (Figure 5C; for quantification, see Figure 5D). In a modified Boyden chamber migration assay, HUVE cells containing the TSAd siRNA showed a dose-dependent decrease in their ability to respond chemotactically to VEGF-A (Figure 5E). In contrast, and in accordance with the lack of effect of the pY951 peptide on VEGF-A-induced mitogenicity (cf. Figure 3C), incorporation of BrdU in response to VEGF-A was not affected by introduction of TSAd siRNA (Figure 5F). Combined with the data in Figure 3, these results strongly indicate that VEGF-A-induced Y951 phosphorylation and coupling to TSAd is critical for organization of the actin cytoskeleton and for migration, but not proliferation, of endothelial cells.

Expression and function of TSAd in tumor vasculature

TSAd expression in intact vessels has not been analyzed previously. Immunofluorescent analysis showed colocalization of TSAd and VEGFR-2 in vessel-like structures in day 8 EBs (Figure 6A). To examine whether TSAd was expressed at other sites of active angiogenesis, human kidney tumor sections were stained with affinity-purified anti-TSAd antibodies together with FITC-conjugated Ulex Europaeus Agglutinin-1 (UEA-1), a well-established marker for human endothelial cells. Figure 6B shows that TSAd was expressed in the tumor vasculature (top panel), as well as in vessels in the adjacent fibrotic kidney tissue (middle panel) and in normal kidney vessels (bottom panel).

To examine the role of phosphorylated Y951-TSAd in an *in vivo* model of pathological angiogenesis, T241 fibrosarcoma growth was examined in TSAd-deficient mice ($TSAd^{-/-}$) and compared to heterozygous $TSAd^{+/-}$ and Wt C57BL/6 mice. Expansion of solid tumors is known to be limited by the extent of vascularization of the tumor. Indeed, Figure 7A shows that tumor growth was considerably compromised in the knockout animals as well as in the heterozygous $TSAd^{+/-}$ animals. Moreover, vessel density was examined by immunofluorescent staining for expression of CD31 (Figure 7B), which was quantified by counting the number of vessels per microscopic field of tumor sections. Vessel density was clearly reduced in the tumors from homozygous and heterozygous TSAd-deficient animals (Figure 7C). Together, these data indicate that pY951-TSAd signaling downstream of VEGFR-2 is required for efficient tumor vascularization.

Discussion

In recent years, novel therapeutic strategies for treatment of cancer have been developed, based on inhibition of tumor blood vessel formation. It was recently demonstrated that treatment with neutralizing antibodies against VEGF is of clinical benefit for colorectal tumor patients (Yang *et al*, 2003). An alternative and attractive strategy is to block the receptor or its downstream signaling pathways in the responding cell rather than targeting several ligands for the same receptor produced by many different cell types. Potent inhibitors of the VEGFR-2 kinase and related kinases (Boyer, 2002) have proven to be very effective in animal tumor studies. As VEGFR-2 is critical not only for endothelial cell function but also for cellular processes such as neuronal survival (for a review, see Brockington *et al*, 2004), inhibition of specific VEGFR-2-induced signaling pathways may be preferable in long-term treatments. In this study, we provide a pan-phosphorylation site map of VEGFR-2 to serve as a

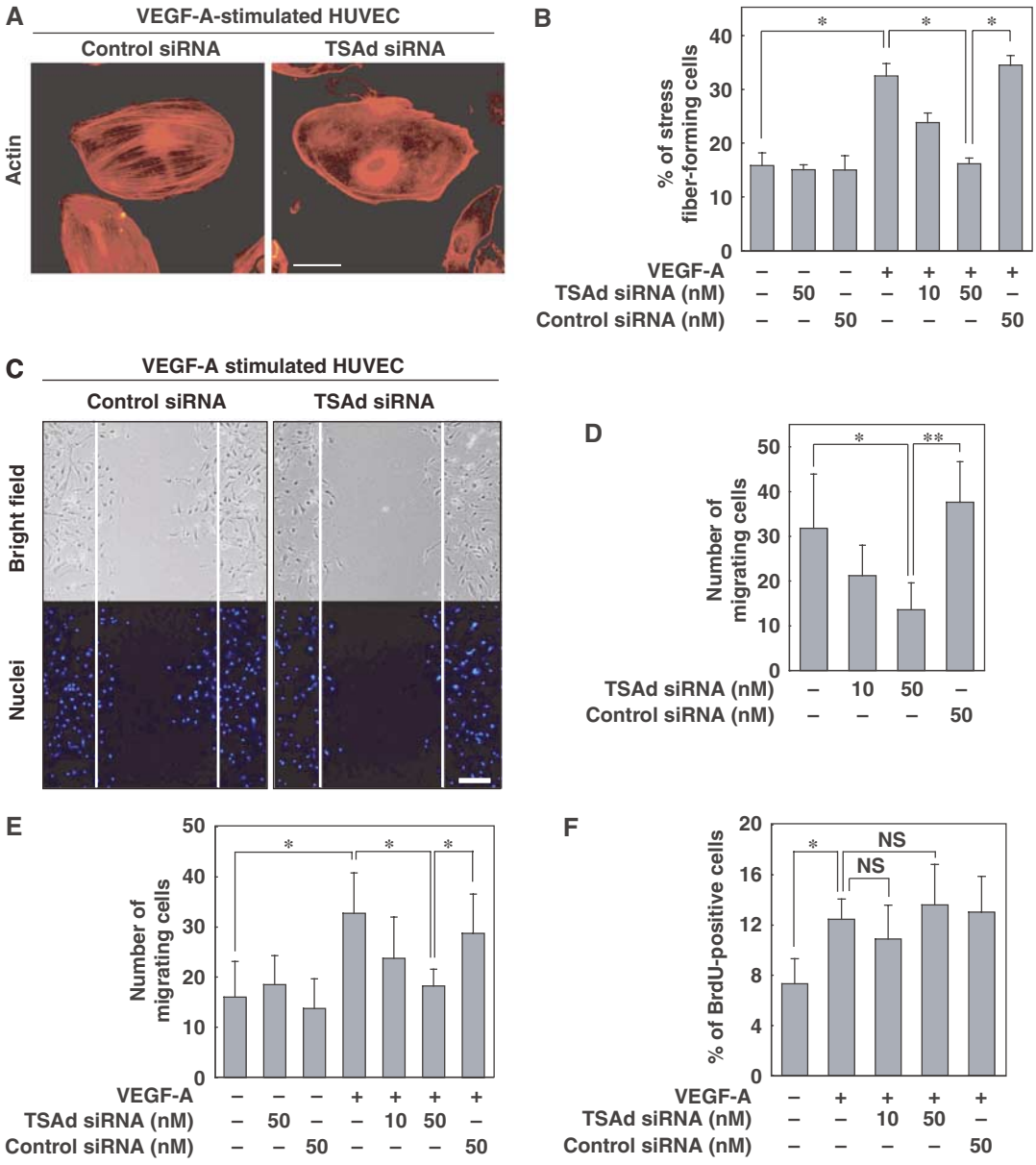

Figure 5 Attenuation of TSAd expression by specific siRNA in HUVE cells leads to a block in VEGF-induced stress fiber formation and motility, but not mitogenesis. (**A**) VEGF-A-induced actin stress fiber formation in HUVE cells transfected with 50 nM TSAd siRNA and control siRNA visualized by TRITC-phalloidin. Bar: 25 μm. (**B**) Quantification of VEGF-A-induced stress fiber formation in cells transfected with different concentrations of TSAd and control siRNA. (**C**) VEGF-A-induced wound closure in HUVE cell monolayer in cells transfected with 50 nM TSAd or control siRNA. Bar: 250 μm. (**D**) Quantification of the VEGF-A-induced migration of cells into the wounded area by HUVE cells transfected with TSAd or control siRNA at indicated concentrations. (**E**) VEGF-A-induced migration in a modified Boyden chamber of HUVE cells transfected with TSAd and control siRNA. (**F**) BrdU incorporation in HUVE cells transfected with TSAd or control siRNA. Similar results were obtained in two independent experiments for each assay. Bars in panels B and D–F show mean ± s.d. of triplicate wells. $*P<0.05$, and $**P<0.01$ (Mann–Whitney *U*-test). NS = not significant.

basis for further development of therapies to block excess angiogenesis in different diseases.

Our data show that relatively few tyrosine residues are used as phosphorylation sites in the VEGFR-2. The chosen condition (electrophoresis at pH 1.9) allows resolution of all possible tryptic peptides derived from human VEGFR-2, except the one containing Y1175 (see Figure 1A). Y1175 in VEGFR-2 is instrumental in VEGF-A-induced endothelial cell proliferation (Takahashi *et al*, 2001). Recent data from the Shibuya group support this notion by showing that replacement of Y1175 with phenylalanine leads to a halt in endothelial cell differentiation and embryonic death (Sakurai *et al*, 2005). Through sequencing individual VEGFR-2 tryptic spots in combination with analyses of individual tyrosine-to-phenylalanine substitutions of all noncatalytic tyrosine residues and selected sites within the kinase domain, we demonstrated phosphorylation of Y951, 1054, and Y1214, but not of Y801, Y822, Y938, Y996, or Y1223. In addition, our data indicate phosphorylation of Y1059 and, at low stoichiometry, the C-terminal Y1305, Y1309, and Y1319. We cannot exclude phosphorylation at other sites but conclude that, if it does occur, the sites are rapidly dephosphorylated or phosphorylation occurs in a very limited number of receptor molecules at any given time point.

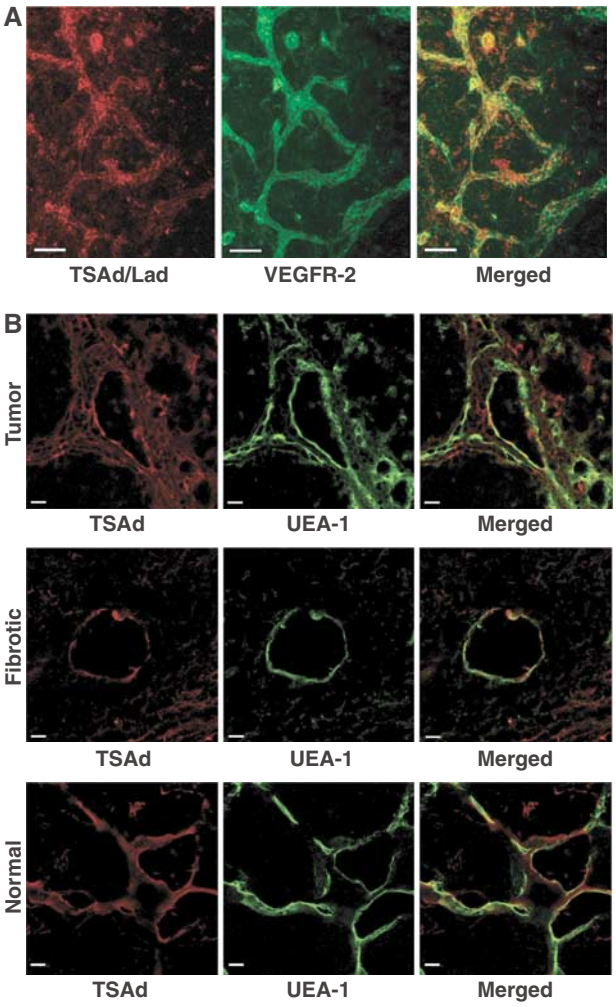

Figure 6 Expression of TSAd in endothelial cells in EBs and in tumor vessels. (**A**) Coexpression of VEGFR-2 and TSAd/Lad in embryonic vessels is shown by immunostaining of whole-mount EBs treated with VEGF-A for 8 days. Bar: 100 μm. (**B**) Expression of TSAd in human kidney tumor vessels (top panel), in vessels in adjacent fibrous kidney tissue (middle panel), and in normal kidney vessels (bottom panel) as visualized by costaining with FITC-labeled UEA-1. Bar: 10 μm.

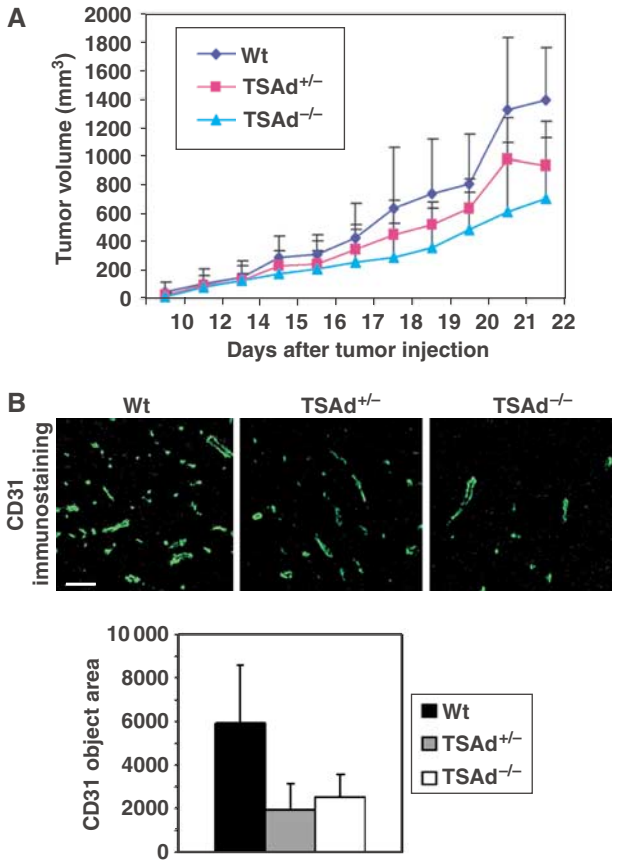

Figure 7 Decreased tumor growth rate and vascularization in $TSAd^{-/-}$ mice. (**A**) Tumor growth over time in C57BL/6 Wt ($n=5$), $TSAd^{+/-}$ ($n=4$), and $TSAd^{-/-}$ ($n=10$) mice after injection of T241 fibrosarcoma cells (day 0). Error bars indicate the s.d. (**B**) Upper panel, visualization of vessels in C57BL/6 Wt, $TSAd^{+/-}$, and $TSAd^{-/-}$ mice by staining for CD31. Bar: 100 μm. Lower panel, quantification of CD31-positive vessel area in sections from tumors from C57BL/6 Wt, $TSAd^{+/-}$, and $TSAd^{-/-}$ mice. Error bars indicate the s.d.

Using phosphosite-specific antibodies, we show that Y951 is phosphorylated in some but not all endothelial cells expressing VEGFR-2. In contrast, Y1175 and Y1214 were phosphorylated in all VEGFR-2-positive cells. Therefore, Y951 may be subject to regulated phosphorylation or dephosphorylation in certain endothelial cells, or the conformation—and therefore the accessibility of Y951 as a substrate—may vary in different cells. The conformation of VEGFR-2 could be affected, for example, by coreceptors for VEGFR-2 such as heparan sulfate, neuropilins, or integrins (Matsumoto and Claesson-Welsh, 2001), which may be differentially expressed in endothelial cells. Alternatively, Y951 is not phosphorylated directly by VEGFR-2, but by a differentially expressed kinase. Interestingly, phosphorylation of Y951 in endothelial cells in EB vessels was more pronounced in vessel structures lacking associated pericytes. Resting capillaries are characterized by a pericyte coat, whereas pericytes are displaced from vessels undergoing active angiogenesis. It is possible that pY951-dependent signal transduction is dispensable in the mature vessel but required during active angiogenesis.

Furthermore, we show that phosphorylation of Y951 and coupling to TSAd regulate actin reorganization and cell migration, but not mitogenicity in response to VEGF-A. Thus, we have confirmed and extended previous findings showing the requirement of Y951 in cellular migration (Zeng *et al*, 2001). TSAd, which is tyrosine phosphorylated in response to VEGF treatment of primary endothelial cells, formed a transient complex with Src. The involvement of Src in actin reorganization and cell migration is well established (for a review, see Frame, 2004). On the other hand, we did not find a role for the pY951–TSAd–Src pathway in cell proliferation based on a BrdU incorporation assay either using cells transfected with pY951 peptide or TSAd siRNA. We showed that the peptide was not subject to rapid degradation or dephosphorylation (see online supplementary data), but we cannot exclude that the longer duration of the BrdU assay compared to the actin stress fiber and migration assays allowed escape from the suppressive effect of the peptide on the pY951–TSAd–Src pathway. However, the stability of the siRNA during the time course of the BrdU assay is long enough (up to 6 days; data not shown) to allow firm

conclusions, and in combination the two strategies show a specific requirement for the novel pathway in endothelial cell migration.

TSAd contains an Src homology 2 (SH2) domain and a proline-rich domain allowing SH3-dependent interactions. TSAd has also been designated as VRAP and has been shown by yeast two-hybrid methodology to couple to Y951 (Wu *et al*, 2000). TSAd has been reported to bind to PLCγ1 and PI3-kinase, probably through the proline-rich domain interacting with the SH3 domain in PLCγ1 and PI3-kinase (Wu *et al*, 2000). However, these and other pathways previously implicated in growth factor-regulated actin reorganization, such as the ERK and p38 MAPK pathways, were still induced in response to VEGF-A treatment of cells expressing a Y951F VEGFR-2 substitution (data not shown). The murine counterpart to TSAd, designated LAD/RIBP, was initially identified as a binding partner for specific Src and Tec family kinases involved in T-cell receptor signaling (Choi *et al*, 1999; Rajagopal *et al*, 1999). Targeted disruption of the *TSAd/LAD/RIBP* gene in mice does not cause major developmental abnormalities, but activation of the T-cell receptor is impaired, leading to immune-response deficiency (Rajagopal *et al*, 1999). Vasculogenesis and angiogenesis during development of the $TSAd^{-/-}$ mice have not been examined, but, as the mice survive birth and have a normal lifespan, there are most likely no major complications. Our data on decreased tumor growth and vascularization in the TSAd knockout mice (Figure 7) implicate the pY951–TSAd pathway in pathological angiogenesis. It has been demonstrated that different molecular mechanisms operate during vasculogenesis and angiogenesis and that deregulated pathological angiogenesis may impose extreme demands on the organism. Thus, inactivation of the placenta growth factor (*PLGF*) gene is compatible with normal development, but leads to impaired angiogenesis, plasma extravasation, and collateral growth during ischemia, inflammation, wound healing, and cancer (Carmeliet *et al*, 2001).

Actin reorganization is instrumental in the formation of a new vessel. Migration of the cells and organization into a lumen-containing, connecting tubule require dramatic changes in the cell shape. Multiple pathways appear to regulate actin reorganization and endothelial cell migration. Thus, VEGF-A-induced cell migration has been shown to occur by heterotrimeric Gq11 in PI3-kinase-independent activation of RhoA (Zeng *et al*, 2002), by the coupling of Shb to FAK and PI3-kinase via Y1175 in VEGFR-2 (Holmqvist *et al*, 2004), and by activation of cdc42 and p38 MAPK via Y1214 in a Rac/Rho-independent manner (Lamalice *et al*, 2004). Using multiple assays to examine the consequence of blocking either Y951 phosphorylation and TSAd expression, we have constructed a novel pathway downstream of VEGFR-2 that is critical for migration but not proliferation of endothelial cells in response to VEGF-A. Our studies suggest the involvement of pY951-TSAd in tumor angiogenesis and indicate their usefulness as targets in future development of antiangiogenic strategies.

Materials and methods

Tissue culture

Human 293T cells used for transient expression of VEGFR-2 were maintained in Dulbecco's modified Eagle's medium (DMEM, Invitrogen) and 10% fetal calf serum (FCS). Primary HUVE cells (Clonetics), passage 6–10, were cultured on 0.5% gelatin-coated plastic in EBM MV2 (Promocell) or in MCDB131 (Invitrogen) and 10% FCS/10 ng/ml FGF-2 (Peprotech). Murine embryonic stem (ES) cells (R1; strain SVJ 129) were kindly provided by Dr A Nagy, Mount Sinai Hospital, Ontario, Canada. Undifferentiated ES cells were cultured on mitomycin C-treated mouse embryonic fibroblasts in DMEM, 15% FCS, 25 mM HEPES, and 1.2 mM sodium pyruvate (Invitrogen), 19 μM monothioglycerol (Sigma-Aldrich), and 1000 U/ml LIF (Chemicon International). Human kidney tumor tissue in 6-μm sections was obtained from the Fresh Tissue Biobank at Uppsala University Hospital and used with the permission of the medical ethics commission of the University of Uppsala. T241 fibrosarcoma cells used for tumor challenge in mice, and PAE cells expressing Wt or mutant VEGFR-2, were maintained in DMEM and 10% FCS.

Antibodies

Rat anti-mouse CD31, rat anti-mouse VEGFR-2 (Flk-1), and FITC-conjugated monoclonal anti-BrdU were obtained from BD Biosciences; rabbit anti-phospho-VEGFR-2 (Y951, Y1175, and Y1214) were from Cell Signaling Technology Inc. Rabbit anti-VEGFR-2, affinity-purified rabbit anti-Src (human/mouse sequence), and rabbit anti-phosphotyrosine PY20 and PY99 were from Santa Cruz Biotechnology, Inc. Mouse monoclonal anti-phosphotyrosine 4G10 (#05-321) was from Upstate Biotechnology. Rabbit polyclonal anti-ASMA antibody was from Lab Vision Corp. The rabbit antiserum was raised in-house against the kinase insert domain of VEGFR-2. The anti-Lad antibody was raised against the 19 C-terminal amino-acid residues 348–366 in murine TSAs/Lad. The antibody against human TSAd has been described (Sundvold *et al*, 2000).

Site-directed mutagenesis

Human VEGFR-2 cDNA in the pCDNA3.1 vector was used in PCR site-directed mutagenesis (QuikChange XL site-directed mutagenesis kit, Stratagene) to replace tyrosine codons with phenyl alanine codons. See the supplement for primer sequences. All mutations were verified by DNA sequencing. The construction of VEGFR-2/CT5 truncation and generation of PAE cells expressing VEGFR-2 Wt and mutant versions have been described (Qi and Claesson-Welsh, 2001).

Immunocomplex kinase assay and two-dimensional phosphopeptide mapping

293T cells (6×10^5) were transfected with Wt or mutant VEGFR-2, using LipofectAMINE™ (Invitrogen). The cells were serum-starved, treated with 100 ng/ml VEGF-A (Peprotech) for 8 min, and processed for IP and immunocomplex kinase assay as described (Dixelius *et al*, 2003). ^{32}P-labeled samples were resolved by SDS–PAGE, transferred to a nitrocellulose membrane, and analyzed using a Bio-Imager BAS-1800II (Fujifilm). The phosphorylated VEGFR-2 bands, localized by a Bio-Imager scan, were excised from the filter and incubated twice with 1 μg trypsin (Promega) as described previously (Dixelius *et al*, 2003). Released tryptic peptides were dried onto cellulose thin-layer chromatography glass plates (Merck), followed by separation in two dimensions using a Hunter thin-layer electrophoresis apparatus (HTLE-7000; CBS Scientific Co.). First-dimension electrophoresis was performed in pH 1.9 buffer (2.2% formic acid, 7.8% acetic acid in H_2O) for 40 min at 2000 V, and the second dimension ascending thin-layer chromatography was performed in isobutyric acid buffer (62.5% isobutyric acid, 1.9% n-butyl alcohol, 4.8% pyridine, and 2.9% acetic acid in H_2O) overnight. The separated ^{32}P-labeled peptides were visualized using the Bio-Imager, and peptide spots of interest were scraped off the plates and eluted by incubation in 20% acetonitrile. Part of the extract (25–100 c.p.m.) was lyophilized and hydrolyzed in 6 M HCl for 1 h at 110°C and subjected to phosphoamino-acid analysis (Ito *et al*, 1998). The remaining phosphopeptide sample was sequenced by Edman degradation using a gas-phase sequencer (Applied Biosystems). In all, 20 sequencing cycles were collected, dried, and analyzed for their content of ^{32}P-radioactivity using the Bio-Imager.

Immunofluorescent staining of EBs and tumors

Induction of angiogenesis in mouse EBs was described previously (Magnusson *et al*, 2004). Briefly, dissociated ES cells were cultured in the presence of 20 ng/ml VEGF-A in hanging drops (1200 cells/20 μl medium without LIF; denoted day 0) to induce aggregation. After 4 days, EBs were plated individually in eight-well culture

slides (BD Falcon) in the presence of VEGF-A. On day 8, EBs were treated with fresh VEGF-A for 30 min and fixed and incubated with primary antibodies as indicated, followed by appropriate secondary antibodies. Coverslips were mounted using Fluoromount-G (Southern Biotechnology Associates) and examined using a Nikon Eclipse E1000 microscope. For detection of TSAd in human vasculature, 6 μm sections of human kidney tumor tissue (obtained from the Fresh Tissue Biobank, Uppsala University Hospital) were incubated with anti-TSAd antibodies, followed by incubation with anti-rabbit-Fab2-Alexa-568 (Invitrogen). Endothelial cells were detected using FITC-conjugated UEA-1 (Vector laboratories). Samples were examined using an LSM 510 META confocal microscope (Carl Zeiss).

Detection of stress fiber formation

HUVE cells on culture slides were serum-starved in MCDB131/5% FCS and transfected with 3 μg of biotin-labeled synthetic VEGFR-2 peptides, phosphorylated or not (biotin-CRQGKD (p)Y951VGAIPV-OH, biotin-CRQGKDY951VGAIPV-OH; AnaSpec Inc.), using the HVJ envelope Vector Kit GenomONE (Ishihara Sangyo Kaisha). After 1 h incubation, cells were treated with 50 ng/ml VEGF-A for 15 min at 37°C, fixed in 3% paraformaldehyde in PBS, and permeabilized in 0.2% Triton X-100 in PBS for 45 min. Cells were incubated in blocking buffer (10% goat serum/1% BSA in PBS), and subsequently in the presence of FITC-conjugated streptavidin (BD Biosciences), washed and incubated with 10 μg/ml TRITC-labeled phalloidin (Sigma-Aldrich) for 45 min at RT, washed again, and incubated with 5 μg/ml Hoechst 33342 (Invitrogen). The percentage of stress fiber-forming cells/total cells was calculated from five fields (× 20 objective) per well.

Detection of S-phase cells

HUVE cells were serum-starved in MCDB131/0.5% FBS for 24 h, transfected or not with 3 μg of pY951 or Y951 peptides for 1 h 30 min, followed by addition of 50 ng/ml VEGF-A or medium. After 20 h incubation at 37°C, 10 μM BrdU (Sigma-Aldrich) was added, and incubation continued for 4 h. Cells were fixed in 70% ethanol for 30 min, washed with PBS, and incubated in 0.02 M NaOH for 2 min, followed by five washes with PBS. FITC-conjugated anti-BrdU monoclonal antibody (2:5 dilution) was added, and after 1 h the cells were stained with 5 μg/ml Hoechst 33342. The labeling index was expressed as the percentage of labeled nuclei/total nuclei from five fields (× 20 objective) per well.

Wound assay

Monolayers of HUVE cells untreated or transduced with retrovirus expressing the EGF receptor/VEGFR-2 chimera (Wt or Y951F EGDR; the construction or retroviruses and the characteristics of the chimeric receptors have been described before in Zeng *et al*, 2001) were scratched with a universal blue pipette tip and incubated for 24 h in the presence of 50 ng/ml EGF or 20 ng/ml VEGF-A, as indicated. Thymidine (10 μM; Sigma-Aldrich) was included during the incubation to inhibit cell proliferation. Cells were fixed in 4% paraformaldehyde, stained with 5 μg/ml Hoechst 33342 to visualize nuclei, and photographed. Hoechst-positive nuclei that had moved into the wounded area were counted in five fields per well. The mean and s.d. from triplicate wells were determined.

SiRNA-mediated attenuation of TSAd expression

SiRNA against the human TSAd sequence 5′-GGA CCG AAG AAU CAA ACU U tt-3′, antisense 5′-AAG UUU GAU UCU UCG GUC C tc-3′, and a scrambled control (Ambion) were used for transfection of serum-starved HUVE cells, using the HVJ envelope Vector Kit GenomONE. After 18 h incubation, cells were treated without or with VEGF-A, and stained using TRITC-labeled phalloidin to visualize actin stress fibers. The percentage of stress fiber-forming cells/total cells was calculated from five fields (× 20 objective)/well. Migration of cells in a modified Boyden chamber with collagen I-coated micropore (8 μm) polycarbonate filters (Neuro Probe Inc.) was performed as described (Holmqvist *et al*, 2004). Wound assay and BrdU incorporation in HUVE cells transfected with TSAd or control siRNA was performed as described above.

Animal study

TSAd/RIBP/LAD$^{-/-}$ mice were generated by homologous recombination (Rajagopal *et al*, 1999) and backcrossed into a C57BL/6 mice background (kindly provided by Professor JA Bluestone, University of Chicago). C57BL/6 TSAd-deficient mice were intercrossed with C57BL/6 mice (Animal Facility, University of Oslo) to generate littermate C57BL/6 Wt, *TSAd*$^{+/-}$, and *TSAd*$^{-/-}$ mice. The animal experiment was approved by the Experimental Animal Board under the Ministry of Agriculture of Norway and conducted in conformity with The Norwegian Regulations on Animal Experimentation and The European Convention for the Protection of Vertebrate Animals used for Experimental and Other Scientific Purposes. The mice were anesthetized with isoflurane (Forene; Abbott) during all manipulations. Mice, 5- to 7-week old, were injected with 0.5×10^6 T241 fibrosarcoma cells (derived from and thus immunologically compatible with C57BL/6 mice) s.c. into the left flank. The tumors were measured with a caliper once a day in a blind procedure, and volumes were calculated by the formula $\pi/6 \times \text{width}^2 \times \text{length}$. Outlayers were included in the statistical analyses presented in Figure 7. At 22 days after tumor cell injection, the mice were killed. Tumors were excised, snap frozen in isopentane/dry ice and cryosectioned, generating 10-μm-thick sections. After immunostaining for CD31, the area of CD31-positive vessels in three individual tumors from each group was quantified with the Easy Image Analysis 2000 program (Tekno Optik) (Magnusson *et al*, 2004). Compensation for background was performed to avoid quantification of unspecific staining. Two sections from different parts of the tumor (center and periphery) were selected, and all CD31-positive vessels in the tumor sections were counted and related to section area.

Supplementary data

Supplementary data are available at *The EMBO Journal* Online.

Acknowledgements

This study was supported by grants from the Swedish Cancer Foundation (project no. 3820-B01-06XAC) and the Novo Nordisk Foundation to Lena Claesson-Welsh and, in part, by National Institute of Health grants HL70567 and HL072178 to Debabrata Mukhopadhyay. Taro Matsumoto was supported in part by a Grant-in-Aid for the High-Tech Research Center from the Ministry of Education, Science, Sports, and Culture of Japan to Nihon University (1550863). Svante Bohman was supported by the Gustav Adolf Johansson Foundation. Tone Berge was supported by a start-up grant to Anne Spurkland from the Medical Faculty, University of Oslo. Anna Dimberg was supported by the Association for International Cancer Research and the Swedish Cancer Foundation (project no. 4828-B03-01PAA). We thank Simin Tahmasebpoor, Dr Johan Botling, and Dr Erik Larsson at the Uppsala University Hospital for advice and discussions and for providing tissues from the Fresh Tissue Biobank (supported by the SWEGENE/Wallenberg Consortium North Biobanking Programme), and Dr Ivar Walaas for providing the C57BL/6 mice.

References

Boyer SJ (2002) Small molecule inhibitors of KDR (VEGFR-2) kinase: an overview of structure activity relationships. *Curr Top Med Chem* **2:** 973–1000

Brockington A, Lewis C, Wharton S, Shaw PJ (2004) Vascular endothelial growth factor and the nervous system. *Neuropathol Appl Neurobiol* **30:** 427–446

Carmeliet P, Moons L, Luttun A, Vincenti V, Compernolle V, De Mol M, Wu Y, Bono F, Devy L, Beck H, Scholz D, Acker T, DiPalma T, Dewerchin M, Noel A, Stalmans I, Barra A, Blacher S, Vandendriessche T, Ponten A, Eriksson U, Plate KH, Foidart JM, Schaper W, Charnock-Jones DS, Hicklin DJ, Herbert JM, Collen D, Persico MG (2001) Synergism between vascular endothelial

growth factor and placental growth factor contributes to angiogenesis and plasma extravasation in pathological conditions. *Nat Med* **7:** 575–583

Choi YB, Kim CK, Yun Y (1999) Lad, an adapter protein interacting with the SH2 domain of p56lck, is required for T cell activation. *J Immunol* **163:** 5242–5249

Dixelius J, Makinen T, Wirzenius M, Karkkainen MJ, Wernstedt C, Alitalo K, Claesson-Welsh L (2003) Ligand-induced vascular endothelial growth factor receptor-3 (VEGFR-3) heterodimerization with VEGFR-2 in primary lymphatic endothelial cells regulates tyrosine phosphorylation sites. *J Biol Chem* **278:** 40973–40979

Dougher M, Terman BI (1999) Autophosphorylation of KDR in the kinase domain is required for maximal VEGF-stimulated kinase activity and receptor internalization. *Oncogene* **18:** 1619–1627

Dougher-Vermazen M, Hulmes JD, Bohlen P, Terman BI (1994) Biological activity and phosphorylation sites of the bacterially expressed cytosolic domain of the KDR VEGF-receptor. *Biochem Biophys Res Commun* **205:** 728–738

Ferrara N (2002) Role of vascular endothelial growth factor in physiologic and pathologic angiogenesis: therapeutic implications. *Semin Oncol* **29:** 10–14

Frame MC (2004) Newest findings on the oldest oncogene; how activated src does it. *J Cell Sci* **117:** 989–998

Hanahan D, Folkman J (1996) Patterns and emerging mechanisms of the angiogenic switch during tumorigenesis. *Cell* **86:** 353–364

Holmqvist K, Cross MJ, Rolny C, Hagerkvist R, Rahimi N, Matsumoto T, Claesson-Welsh L, Welsh M (2004) The adaptor protein shb binds to tyrosine 1175 in vascular endothelial growth factor (VEGF) receptor-2 and regulates VEGF-dependent cellular migration. *J Biol Chem* **279:** 22267–22275

Ito N, Wernstedt C, Engstrom U, Claesson-Welsh L (1998) Identification of vascular endothelial growth factor receptor-1 tyrosine phosphorylation sites and binding of SH2 domain-containing molecules. *J Biol Chem* **273:** 23410–23418

Kabrun N, Buhring HJ, Choi K, Ullrich A, Risau W, Keller G (1997) Flk-1 expression defines a population of early embryonic hematopoietic precursors. *Development* **124:** 2039–2048

Kendall RL, Rutledge RZ, Mao X, Tebben AJ, Hungate RW, Thomas KA (1999) Vascular endothelial growth factor receptor KDR tyrosine kinase activity is increased by autophosphorylation of two activation loop tyrosine residues. *J Biol Chem* **274:** 6453–6460

Lamalice L, Houle F, Jourdan G, Huot J (2004) Phosphorylation of tyrosine 1214 on VEGFR2 is required for VEGF-induced activation of Cdc42 upstream of SAPK2/p38. *Oncogene* **23:** 434–445

Magnusson P, Rolny C, Jakobsson L, Wikner C, Wu Y, Hicklin DJ, Claesson-Welsh L (2004) Deregulation of Flk-1/vascular endothelial growth factor receptor-2 in fibroblast growth factor receptor-1-deficient vascular stem cell development. *J Cell Sci* **117:** 1513–1523

Matsumoto T, Claesson-Welsh L (2001) VEGF receptor signal transduction. *Sci STKE* **2001:** RE21

Qi JH, Claesson-Welsh L (2001) VEGF-induced activation of phosphoinositide 3-kinase is dependent on focal adhesion kinase. *Exp Cell Res* **263:** 173–182

Rajagopal K, Sommers CL, Decker DC, Mitchell EO, Korthauer U, Sperling AI, Kozak CA, Love PE, Bluestone JA (1999) RIBP, a novel Rlk/Txk- and itk-binding adaptor protein that regulates T cell activation. *J Exp Med* **190:** 1657–1668

Sakurai Y, Ohgimoto K, Kataoka Y, Yoshida N, Shibuya M (2005) Essential role of Flk-1 (VEGF receptor 2) tyrosine residue 1173 in vasculogenesis in mice. *Proc Natl Acad Sci USA* **102:** 1076–1081

Spurkland A, Brinchmann JE, Markussen G, Pedeutour F, Munthe E, Lea T, Vartdal F, Aasheim HC (1998) Molecular cloning of a T cell-specific adapter protein (TSAd) containing an Src homology (SH) 2 domain and putative SH3 and phosphotyrosine binding sites. *J Biol Chem* **273:** 4539–4546

Sundvold V, Torgersen KM, Post NH, Marti F, King PD, Rottingen JA, Spurkland A, Lea T (2000) T cell-specific adapter protein inhibits T cell activation by modulating Lck activity. *J Immunol* **165:** 2927–2931

Takahashi T, Yamaguchi S, Chida K, Shibuya M (2001) A single autophosphorylation site on KDR/Flk-1 is essential for VEGF-A-dependent activation of PLC-gamma and DNA synthesis in vascular endothelial cells. *EMBO J* **20:** 2768–2778

Wu LW, Mayo LD, Dunbar JD, Kessler KM, Ozes ON, Warren RS, Donner DB (2000) VRAP is an adaptor protein that binds KDR, a receptor for vascular endothelial cell growth factor. *J Biol Chem* **275:** 6059–6062

Yang JC, Haworth L, Sherry RM, Hwu P, Schwartzentruber DJ, Topalian SL, Steinberg SM, Chen HX, Rosenberg SA (2003) A randomized trial of bevacizumab, an anti-vascular endothelial growth factor antibody, for metastatic renal cancer. *N Engl J Med* **349:** 427–434

Zeng H, Sanyal S, Mukhopadhyay D (2001) Tyrosine residues 951 and 1059 of vascular endothelial growth factor receptor-2 (KDR) are essential for vascular permeability factor/vascular endothelial growth factor-induced endothelium migration and proliferation, respectively. *J Biol Chem* **276:** 32714–32719

Zeng H, Zhao D, Mukhopadhyay D (2002) KDR stimulates endothelial cell migration through heterotrimeric G protein Gq/11-mediated activation of a small GTPase RhoA. *J Biol Chem* **277:** 46791–46798